

Intelligent Link Adaptation for Grant-Free Access Cellular Networks: A Distributed Deep Reinforcement Learning Approach

Joao V. C. Evangelista, *Student Member, IEEE*, Zeeshan Sattar, *Member, IEEE*, Georges Kaddoum, *Senior Member, IEEE*, Bassant Selim, *Member, IEEE*, and Aydin Sarraf

Abstract—With the continuous growth of machine-type devices (MTDs), it is expected that massive machine-type communication (mMTC) will be the dominant form of traffic in future wireless networks. Applications based on this technology, have fundamentally different traffic characteristics from human-to-human (H2H) communication, which involves a relatively small number of devices transmitting large packets consistently. Conversely, in mMTC applications, a very large number of MTDs transmit small packets sporadically. Therefore, conventional grant-based access schemes commonly adopted for H2H service, are not suitable for mMTC, as they incur in a large overhead associated with the channel request procedure. We propose three grant-free distributed optimization architectures that are able to significantly minimize the average power consumption of the network. The problem of physical layer (PHY) and medium access control (MAC) optimization in grant-free random access transmission is modeled as a partially observable stochastic game (POSG) aimed at minimizing the average transmit power under a per-device delay constraint. The results show that the proposed architectures are able to achieve significantly less average latency than a baseline, while spending less power. Moreover, the proposed architectures are more robust than the baseline, as they present less variance in the performance for different system realizations.

Index Terms—grant-free, mMTC, multiple access, reinforcement learning, distributed optimization

I. INTRODUCTION

THE rapid growth of the Internet of Things (IoT), autonomous vehicles, smart grids, and other technologies propelled machine-to-machine (M2M) communications into one of the dominant applications in cellular networks [1]. Machine communication have fundamentally different traffic patterns compared to human-to-human (H2H) ones. In H2H, a few users consume and produce large quantities of data, whereas in M2M applications a large number of devices generate small amounts of data with diverse quality of service (QoS) requirements [1]. Given this difference, the grant-based

transmission approach adopted by current cellular standards is inefficient in the massive machine-type communication (mMTC) scenario [2].

A considerable amount of the devices using the mMTC service are battery powered, whereas in currently deployed wireless systems, a lot of the energy consumed by communicating devices is used for establishing and maintaining connections. As identified in [3], when transmitting small packets, the grant request procedure can result in a significant overhead. While the semi-persistent connection, as adopted by the narrowband internet of things (NB-IoT) standard, might reduce the signaling overhead, it can only do so efficiently in the case of periodic traffic arrival [4]. The specifications of 5G new radio (NR) introduced the two-step random access procedure (in the rest of this work referred to as grant-free access) [5], which allows the users of the network to transmit their data directly on the random access channel (RACH) as opposed to the traditional four-step channel request approach used in long term evolution (LTE) (in the rest of this work referred to as grant-based access). This flexibility with regards to the random access mechanism gives us the opportunity to rethink the design of future networks to service M2M communications.

A grant-free access mechanism can enable devices to transmit data in an arrive and-go manner in the next available slot. Unlike the current grant-based access mechanism in the LTE uplink, devices using grant-free transmission need not wait for a specific uplink grant from the base station. Such a scheme is more desirable for the two broad IoT use cases in 5G, namely mMTC and ultra-reliable low-latency communications (URLLC), as it enables reduced transmission latency, smaller signaling overhead due to the simplification of the scheduling procedure, and improved energy efficiency (battery life) of the IoT devices with a reduction in signaling and ON time. Grant-free and semi-grant-free transmission are considered for low latency IoT transmission in [6].

Notwithstanding, in grant-free access, as the transmissions are not scheduled on orthogonal time-frequency resources, there is a high probability that different devices will randomly choose the same resource blocks for uplink transmission, resulting in the superposition of data (collision). The cross-layer optimization of a grant-free network requires consideration of both physical layer (PHY) and medium access control (MAC) layer measurements while taking into account their interaction to obtain the relevant performance metrics (e.g.

This work has been submitted to the IEEE for possible publication. Copyright may be transferred without notice, after which this version may no longer be accessible.

Part of this work was done while the first author was an Mitacs Accelerate intern at Ericsson Canada. This research was also sponsored by a FRQNT B2X Scholarship.

J.V.C. Evangelista, G. Kaddoum and Z. Sattar were with the Department of Electrical Engineering, École de Technologie Supérieure, Montreal, QC, H3C 1K3 CA, e-mail: {joao-victor.de-carvalho-evangelista.1, zeeshan.sattar.1}@ens.etsmtl.ca and georges.kaddoum@etsmtl.ca

B. Selim and A. Sarraf were with the Ericsson Canada, Montreal, QC, H4S 0B6 CA, email: {bassant.selim, aydin.sarraf}@ericsson.com

the average power consumption and delay), making it a very challenging problem. Moreover, grant-free transmission poses new challenges in the design of PHY and MAC protocols. In this context, static policies for adaptive modulation and coding (AMC), power control, and packet retransmission are not able to efficiently satisfy the diverse throughput, latency, and power saving requirements of mMTC. Furthermore, due to a lack of scheduling by a central entity in such networks, a distributed optimization approach with partial state information is a natural choice to optimize the network performance while keeping communication overhead to a minimum. In this light, we argue that modeling the problem as a partially observable stochastic game (POSG) and proposing a solution within the multiagent reinforcement learning (MARL) framework is the best approach to this problem. While the POSG model is able to elegantly capture the evolution of the wireless environments and its interactions with the users in time, the MARL framework enables a distributed decision-making solution, balancing short-term and long-term performance goals.

A. Related Work

Random access is an essential component of every multiuser wireless communication system, either as a method of establishing a connection between an user and a base station (BS) (in grant-based systems), or to transmit data (in grant-free systems). Recently, the rise in prominence of mMTC applications has sparked a debate around which of the competing methods should be adopted. A large portion of the research community started advocating for the adoption of a grant-free approach to serve mMTC applications [7], [8]. In [2] an extensive comparison of the performance of grant-free and grant-based systems with and without subcarrier sensing against a variable packet length is presented. The authors concluded that for shorter packet lengths (as expected in mMTC applications) grant-free transmission with sensing results in the best throughput, making a stronger case for grant-free mMTC systems. Moreover, in [9], [10], stochastic geometric models and analytical results for grant-free non-orthogonal multiple access (NOMA) are presented.

In [11], the authors propose an open loop power control scheme with path loss compensation in an uplink grant-free ultra reliable low-latency communication (URLLC) network to minimize the outage probability. They investigate the effects of the path-loss compensation factor and the expected received power on the network outage probability. In [12], the authors introduce a model to abstract multi-packet reception in grant-free networks. They analyze the dynamics of the network and propose a reinforcement learning (RL) approach to determine the amount of resource blocks to allocate to grant-free transmission in order to maximize the normalized throughput. In [13], the effects of pilot selection in a grant-free NOMA system are investigated, and a deep reinforcement learning (DRL) approach is proposed, where each user, without any information exchange, selects its pilots in order to maximize its throughput. Despite their contributions, none of these works address the interactions between the PHY and MAC layers and how to harness their flexibility to improve the overall network performance.

In [14], a reinforcement learning algorithm is proposed to jointly select an AMC, and dynamic power management (DPM), in order to minimize the transmitted power in a single-user system while satisfying a certain delay constraint. Afterwards, in [15] the work in [14] is extended to consider a multiuser system in an IEEE 802.11 network with subcarrier sensing multiple access (CSMA). The authors considered three users contending for channel access, and adopted an independent learners approach [16], where each user optimizes its own rewards, ignoring all interactions with other users. Despite its simplicity, the independent learners solution is known to have several issues such as Pareto-selection, nonstationarity, stochasticity, alter-exploration and shadowed equilibria [17].

Although instructive, none of these works addressed the challenges involved in the distributed cross-layer optimization of the grant-free uplink transmission for mMTC service. Moreover, previous works on this topic have failed to address the issues involved in the massive scale aspect of mMTC applications, despite their contributions. In this manuscript, we propose three distributed solutions based on MARL, ranging from a fully distributed solution to a centralized learning with distributed inference, to minimize the average power consumption of the network while satisfying delay constraints.

B. Contributions

Although instructive, none of these works addressed the challenges involved in the distributed cross-layer optimization of the grant-free uplink transmission for mMTC service. In this manuscript, we propose three distributed solutions based on MARL, ranging from a fully distributed solution to a centralized learning with distributed inference, to minimize the average power consumption of the network while satisfying delay constraints. The contributions of this paper are summarized as:

- We propose a POSG to model the PHY and MAC dynamics of a grant-free mMTC network and to formulate the cross-layer power minimization problem. This model considers the channel and packet generation dynamics, and accommodates machine-type devices (MTDs) with diverse QoS requirements and packet arrival intensities.
- We propose a fully distributed independent learners (IL) architecture, based on the proximal policy optimization (PPO) algorithm [18], to eliminate the all the communication overhead involved in the cross-layer optimization.
- We propose a distributed actors with centralized critic (DACC) architecture where the PPO actor and critic are split and each agent trains its own actor while a single critic is trained by a central entity running on an edge computing node. This architecture achieves a reduced overhead while allowing the possibility of cooperative behavior to arise among the MTDs, in our second scheme. As the central entity is able to aggregate measurements from every user, the critic's loss function is calculated from a global performance measure.
- We propose centralized learning with decentralized inference (CLDI) architecture to eliminate the exponential increase of the policy search space with more MTDs.

In this scheme, every MTD uses the same policy, which is trained on an edge computing node. However, each MTD uses the model in a distributed fashion by making decisions based on local data.

- We provide an extensive analysis of the performance of all three architectures when servicing MTDs with diverse QoS requirements and packet arrival rates. Moreover, we compare their performance with a reactive hybrid automatic repeat request (HARQ) protocol with power boosting as a baseline. Finally, we include a quantitative analysis of the tradeoffs involving the performance and the overhead of the proposed architectures in scenarios with different device deployment densities.

C. Notation

Throughout this paper, italic lowercase letters denote real and complex scalar values. Lower case boldface letters denote vectors, while upper case boldface denote matrices. A lowercase letter with one subscript, x_i , represents the i -th element of the vector \mathbf{x} , while two subscripts $x_{i,j}$ is used to denote the element on the i -th row and j -th column of matrix \mathbf{X} . The operator $E[\cdot]$ denotes the expected value of a random variable. The function $\mathbb{P}(\cdot)$ represents the probability of an event and $\mathbf{x} \sim \mathcal{CN}(\boldsymbol{\mu}, \mathbf{K})$, denotes that \mathbf{x} is a circularly symmetric complex Gaussian random vector, with mean $\boldsymbol{\mu}$ and covariance matrix \mathbf{K} . The notation $x \sim U(\mathcal{X})$ denotes that x is drawn uniformly from the set \mathcal{X} . The indicator function takes an event as argument and is equal to one if the event happens and zero otherwise, and is represented by $\mathbf{1}(\cdot)$. Sets \mathbb{R} and \mathbb{C} and are the sets of real and complex numbers, respectively. The set $\mathbb{B} = \{0, 1\}$ represents the binary numbers. A calligraphic uppercase letter, such as \mathcal{X} , denotes a set and $|\mathcal{X}|$ is its cardinality. Throughout the paper several variables denote quantities related to a particular user at a given moment in time (e.g. $x_{i,t}$ is related to the i -th user on time slot t). To avoid cluttering the notation we drop the subscript related to the time and use it only when indexing a variable over multiple periods of time is necessary.

D. Organization

This paper is organized as follows: In Section II we present the system model, discussing in details the dynamics of the environment introducing the optimization problem we aim to solve. In Section III, we present the three distributed learning architectures proposed in this work. In Section IV, the performance of the three proposed architectures is evaluated and the results are discussed. Finally, in Section V, we summarize the conclusions.

II. SYSTEM MODEL

In this paper, we consider the problem of designing a distributed link adaptation solution for a grant-free access 5G network providing mMTC service. In a grant-free network, there is no guarantee that a transmission attempt is going to be successful. Hence, the usage of a HARQ protocol is essential to guarantee some reliability to the packet transmissions. In the system under analysis, the MTDs use a reactive

HARQ protocol, where after each transmission attempt the device receives either an acknowledgement (ACK) feedback, in case the transmission attempt was successfully decoded, or a negative-acknowledgement (NACK) feedback, in case the transmission attempt could not be decoded [19]. Notice that we choose the reactive HARQ protocol because the alternative protocols require repeating the same data on every transmission attempt, increasing the transmission power per attempt, which goes against our design objective of minimizing the power expenditure in the network.

We consider a network with N_U MTDs and N_B base stations randomly located within a circular area of radius R . The distance between the i -th device and the j -th BS is denoted by $d_{i,j}$. Moreover, each device is associated to its closest BS. We assume there are N_K orthogonal subcarriers reserved for uplink transmission, and N_P orthogonal preambles. In every transmission time interval (TTI) the active devices randomly select one out of the N_P available orthogonal preambles, and one subcarrier out of the N_K available to transmit its data on. The orthogonal preambles are used by the network to detect user activity and estimate the MTDs' channel response. It is worth highlighting that all the variables discussed in this section are associated to a given TTI; However, for notation convenience, we drop the subscript t used to denote a specific TTI. Additionally, if x is a variable at time t we use a prime superscript x' to denote the value of the same variable at $t+1$.

All devices transmit symbols from a quadrature amplitude modulation (QAM) with order $\beta_i \in \{1, \dots, M\}$, where M is the maximum modulation order. Furthermore, before the start of every TTI, each device has the option to turn off its radio to save power. The radio state is represented by the variable $x_i \in \{0, 1\}$, whenever $x_i = 1$, the radio is on and consumes P_{ON} watts plus whatever power used for the transmission, and when $x_i = 0$, the radio is off and spends P_{OFF} watts. If the radio is on, the device attempts to transmit its data on that particular TTI, hence, the user must select a transmission power $p_i \in \mathcal{P} = \{\rho_1, \dots, \rho_{\max}\}$. So, the received signal at the j -th BS on the k -th subcarrier is

$$r_k = \sum_{i=1}^{N_U} x_i \theta_{i,k} \sqrt{p_i} h_{i,j,k} d_{i,j}^{-\alpha/2} u_i + w_k, \quad (1)$$

where $\theta_{i,k} \in \{0, 1\}$ indicates whether user i is transmitting on subcarrier k , $w_k \sim \mathcal{CN}(0, N_0)$ is a circularly symmetric complex normal random variable modeling the additive white Gaussian noise (AWGN) and α is the path loss exponent. The variable u_i is a symbol from a QAM constellation with order β_i and $\|u_i\|^2 = 1$. Moreover, $h_{i,j,k}$ represents the small-scale fading experienced by the i -th user's signal to the j -th BS on the k -th subcarrier. We assume that the channel remains constant during the TTI duration. To model the relationship between subsequent channel realizations we consider a first-order Gauss-Markov small-scale flat fading model [20] where

$$h'_{i,j,k} = \kappa h_{i,j,k} + n_{i,j,k}, \quad (2)$$

where the innovation $n_{i,j,k} \sim \mathcal{CN}(0, 1 - \kappa^2)$ is a circularly symmetric complex normal random variable. The correlation

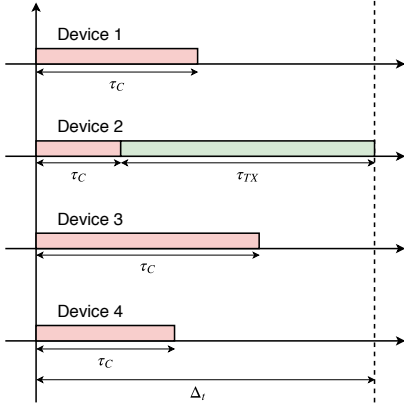


Fig. 1. Illustration of the considered LBT procedure for 4 devices sharing the same channel. The red shaded area represents the random backoff listening time and the green shaded one denotes the transmission time.

between successive fading components is given by [21]

$$\kappa = J_0(2\pi f_{\max}\Delta_t), \quad (3)$$

where f_{\max} is the maximum Doppler frequency, Δ_t is the duration of a single TTI and J_0 is the zero-th order Bessel function of the first kind.

In order to guarantee a harmonious access to the channel and avoid congestion, the system under investigation employs a rate-adaptive listen before talk (LBT) mechanism with random backoff on every subcarrier to control the congestion. This approach is well aligned with the specifications of 5G networks operating on the unlicensed spectrum [22]–[25]. A TTI is divided into two phases: contention and transmission. During the contention phase, the device listens to the channel on a specific subcarrier for a random backoff time $\tau^C < \Delta_t$. If no other user has started transmission during this time, the device starts its transmission for an amount of time $\tau^{TX} = \Delta_t - \tau^C$. The protocol is illustrated in Fig. 1, where we show a situation in which 4 devices are transmitting on the same subcarrier. The red shaded areas indicate the random backoff time τ^C drawn by each user. In this figure, as device 2 drew the smallest backoff time, it takes hold of the channel and transmits its data in the remaining time available in the time slot. In this model, a collision occurs if two devices draw the same random backoff time.

We consider a rate-adaptive congestion control protocol, similar to the one proposed in [15], where a congestion window (CW), given by $CW_{\min}(\beta_i) = \lfloor A2^{M-\beta_i} \rfloor$, where $A \in \mathbb{R}$ is a design parameter, is assigned to the device according to its modulation order. The backoff time of the i -th device is uniformly chosen from $[0, CW_{\min}(\beta_i)]$ and is reset at the end of the time slot.

Definition 1 (Collision): We consider that a collision occurs whenever two devices being served by the same BS select the same preamble and the same subcarrier, and, draw the same random backoff time τ^C .

If a collision occurs, the devices' CW are set to $CW_{\max} = A2^M$. Note that the MTD attempts to transmit

$$z_i = \left\lfloor \frac{\beta_i \tau^{TX}}{LT_S} \right\rfloor \quad (4)$$

packets in a given TTI, where L is the packet length and T_S is the symbol duration. This approach increases the likelihood that a device that intends to transmit at higher rates obtains channel access, avoiding the anomaly identified in [26], where low-rate users significantly degrade the performance of the whole network.

Furthermore, we assume that each device has a packet buffer with a capacity of L_B packets. Let b_i be the number of packets in the i -th device's buffer. We assume that the number of arriving packets follow a Poisson distribution $l_i \sim \text{Poisson}(\lambda_i)$, where λ_i is the mean packet arrival rate. The number of packets departing (the goodput) the device's buffer is denoted by g_i . The goodput of the i -th MTD is a function of the device's transmit power, its selected subcarrier, its channel to the receiving BS, and the interference power at the receiving BS. Let the interference suffered by the i -th MTD's transmission on the k -th subcarrier be

$$I_{i,k} = \sum_{\substack{n=1 \\ n \neq i}}^{N_U} x_n \theta_{n,k} p_n \|h_{n,j,k}\|^2 d_{n,j}^{-\alpha} \quad (5)$$

The probability that the j -th BS decodes a bit transmitted by the i -th MTD in error (denoted as P_i^e) can be approximated by [27]

$$P_i^e \approx \begin{cases} \frac{1}{2} \operatorname{erfc} \left\{ \sqrt{\frac{p_i \|h_{i,j,k}\|^2 d_{i,j}^{-\alpha}}{I_{i,k} + N_0}} \right\} & \text{if } \beta_i = 1 \\ 2 \operatorname{erfc} \left\{ \sqrt{\frac{3 \log_2(\beta_i) p_i \|h_{i,j,k}\|^2 d_{i,j}^{-\alpha}}{2(\beta_i - 1)(I_{i,k} + N_0)}} \right\} & \text{if } \beta_i > 1, \end{cases} \quad (6)$$

Given the approximate probability of decoding a bit in error given in (6), we obtain the probability of losing a packet as

$$P_i^{\text{loss}} = 1 - (1 - P_i^e)^L. \quad (7)$$

Moreover, the number of overflown packets, i.e. packets that arrive while the buffer is full and must be dropped, at the i -th device's buffer is given by

$$\xi_i = \max(b_i + l_i - g_i - L_B, 0). \quad (8)$$

A. Problem Formulation

The main goal of this work is to derive a link adaptation algorithm to minimize the average power consumption over time of the network under a constraint on the average delay. Notice that as the MTDs transmission attempts are not scheduled by a central network the proposed algorithm must run on each device in a distributed fashion. Also, although the goal is to minimize the average power consumption the algorithm has only local information to make decisions on the link adaptation. This problem can be formulated as a POSG [28]. A POSG, models how multiple agents, with distinct and possibly adversarial goals, interact with a stochastic changing environment in discrete time slots. At each time slot, the agents receive a partial, and possibly noisy, observation of the environment and select an action to take in the next slot based on this observation. Each set of actions selected by the agents incurs a cost and the objective of the problem is to find the joint policy that minimizes the cost. In this

work, we are concerned with infinite horizon POSGs [29], as the task we are optimizing cannot be described by finite length episodes. The POSG problem is formally defined by a tuple $(\mathcal{U}, \mathcal{S}, \mathcal{A}, \mathcal{P}_S, c, \mathcal{O})$, where \mathcal{U} is the set of agents, where each MTD out of the N_U total constitutes an agent. \mathcal{S} and $\mathcal{A} = \times_{i \in \mathcal{U}} \mathcal{A}_i$ denote the state space and the joint action space of the system, respectively, where \mathcal{A}_i is the action space of the i -th agent. The state-action transition probability $\mathcal{P}_S : \mathcal{S} \times \mathcal{A} \times \mathcal{S} \rightarrow [0, 1]$ gives the probability $\mathcal{P}(s'|s, \mathbf{a})$ of transitioning to a state s' , given the current state \mathbf{s} and the joint selected action \mathbf{a} . The set $\mathcal{O} = \{\mathcal{O}_i : \mathcal{O}_i \subseteq \mathcal{S} \forall i \in \mathcal{U}\}$ contains the observation space of each device, which is a subset of the complete state space. Furthermore, $c : \mathcal{S} \times \mathcal{A} \rightarrow \mathbb{R}$ is the cost function associated to the problem. The cost function gives the cost of taking action a while on state s .

Definition 2 (Policy): A policy $\pi(a|o)$, for $a \in \mathcal{A}$ and $o \in \mathcal{O}_i$ is a conditional probability distribution that gives the probability that the agent selects the action a given that it observes the local observation o .

The joint policy of all the agents is denoted by $\boldsymbol{\pi} = [\pi_1, \dots, \pi_{N_U}]$. Notice that $\boldsymbol{\pi}$ is also a conditional probability function given by

$$\pi(\mathbf{a}|\mathbf{s}) = \prod_{i=1}^{N_U} \pi_i(a_i|o_i) \quad (9)$$

The optimality criteria defines the optimization objective of the problem. In the case of an infinite-horizon POSG, we want the average cost over time to be minimized. Therefore, a natural optimality criteria for the joint policy $\boldsymbol{\pi}$ is the expected discounted cost [30], which is given by

$$C_{\boldsymbol{\pi}}(\mathbf{s}) = E_{\boldsymbol{\pi}} \left[\sum_{t=0}^{\infty} \gamma^t c(\mathbf{s}_t, \mathbf{a}_t) \mid \mathbf{s}_0 = \mathbf{s} \right], \quad (10)$$

where $0 < \gamma < 1$ is the discount factor. So, the cost function takes into account the effect of the action on the current and future TTIs. The discount factor is necessary to keep the summation in (10) bounded and can be interpreted as how much weight should the agent's decision give to future costs.

Let $\boldsymbol{\Pi} = \{\boldsymbol{\pi} | \boldsymbol{\pi} : \mathcal{A} \times \mathcal{S} \rightarrow [0, 1]\}$ be the set of all possible joint policies. Then, the solution of a POSG is defined as

$$\begin{aligned} \boldsymbol{\pi}^* &= \arg \min_{\boldsymbol{\pi} \in \boldsymbol{\Pi}} E_{\mathbf{s} \sim \mathbb{P}(\mathbf{s})} [C_{\boldsymbol{\pi}}(\mathbf{s}) | \mathbf{s}_0 = \mathbf{s}] \\ &= \arg \min_{\boldsymbol{\pi} \in \boldsymbol{\Pi}} E_{\mathbf{s} \sim \mathbb{P}(\mathbf{s}), \boldsymbol{\pi}} \left[\sum_{t=0}^{\infty} \gamma^t c(\mathbf{s}_t, \mathbf{a}_t) \mid \mathbf{s}_0 = \mathbf{s} \right], \end{aligned} \quad (11)$$

where $\mathbb{P}(\mathbf{s})$ is the probability distribution over the set of states \mathcal{S} while following the joint policy $\boldsymbol{\pi}$, and, $\boldsymbol{\pi}^*$ is the policy that minimizes the expected discounted cost from the set of all possible policies. The problem in (11) is known to be undecidable, meaning that given a threshold, it is not possible to tell whether there exists a policy that has an expected discounted cost smaller than the threshold [31]; However, as we show in Section III, we can reformulate the problem in (11) to a proxy problem, and approximate the policies π_i by a parametric function approximator $\pi_{\mathbf{w}_i}$, where \mathbf{w}_i is the set of parameters for the device's policy. Consequently, the set of all

possible joint policies $\boldsymbol{\Pi}$ becomes constrained to the set of all possible policies that can be approximated by the parametric model. Considering a differentiable parametric model, we can use a data-driven learning approach to optimize the parameters and obtain high-quality sub-optimal solutions to (11).

The cellular system model described so far can be conveniently mapped into the POSG problem formulation. The state of the system can be denoted by

$$\mathbf{s} = (\mathbf{h}, \mathbf{b}, \mathbf{l}, \mathbf{g}), \quad (12)$$

where $\mathbf{h} = \text{vec}([\mathbf{H}_1, \dots, \mathbf{H}_{N_U}])$ and $\mathbf{H}_i = [||h_{i,j,k}||^2 d_{i,j}^{-\alpha}]_{j,k}$ is a $(N_B \times N_S)$ matrix where each entry is the channel gain between the i -th MTD and the j -th BS on the k -th subcarrier. Additionally, \mathbf{b} , \mathbf{l} , and \mathbf{g} are vectors containing the number of packets in the buffer, the number of arriving packets and the goodput of each MTD, respectively. As the devices only have access to their local information the observation vector is given as

$$\mathbf{o}_i = [\text{vec}(\mathbf{H}_i), x_i, b_i, l_i, g_i]. \quad (13)$$

Furthermore, we map the optimization variables of the power minimization problems into the joint action vector as

$$\mathbf{a} = (\boldsymbol{\theta}, \boldsymbol{\beta}, \mathbf{p}, \mathbf{x}), \quad (14)$$

where $\boldsymbol{\theta} = [\theta_1, \dots, \theta_{N_U}]$ and $\theta_i \in \{0, 1\}^{N_S}$ is the subcarrier selection vector of the i -th user, and, $\sum_{k=1}^{N_S} \theta_{i,k} \leq 1$. Also, $\boldsymbol{\beta}$, \mathbf{p} , \mathbf{x} correspond to the modulation order, power and radio state selected by each MTD, respectively.

In this work, we want to minimize the power usage subject to a latency constraint. The POSG problem formulation is not compatible with a constrained objective. Hence, we follow the approach in [32] to model constrained Markov decision processes (CMDPs) and augment the objective function with a Lagrangian penalty [33]. Furthermore, according to Little's theorem [34], the average number of packets queued in the buffer is proportional to the average packet delay in queues with stable buffers (i.e. no overflow). Hence, we design the cost function to discourage large number of packets in the queue, which we refer to as the holding cost, while simultaneously penalizing dropped packets, which we refer to as the overflow cost. Therefore, in the POSG formulation, the cost function is

$$\begin{aligned} c(\mathbf{s}, \mathbf{a}) &= \sum_{i=1}^{N_U} \underbrace{x_i(P_{ON} + p_i) + (1 - x_i)P_{OFF}}_{\text{power cost}} + \\ &\quad \omega_i \left(\underbrace{b_i}_{\text{holding cost}} + \underbrace{\mu \xi_i}_{\text{overflow cost}} \right), \end{aligned} \quad (15)$$

where ω_i is a Lagrange multiplier. Thus, if the i -th MTD has a delay constraint equal to δ_i , then, $\omega_i \propto \max(0, [b_i + \mu \xi_i] - \delta_i)$ is proportional to how much the delay constraint is being violated. Moreover, μ is the overflow penalty factor. The overflow penalty factor must be chosen such that dropping packets is sub-optimal, while encouraging devices to transmit with low-power. To meet these requirements, we choose a value of μ such that dropping a packet costs as much as the

largest possible discounted expected cost incurred by holding a packet in the buffer, which happens if the packet is held in the buffer forever. Therefore

$$\mu = \sum_{t=0}^{\infty} \gamma^{t+1} = \frac{\gamma}{1-\gamma}. \quad (16)$$

III. DISTRIBUTED LEARNING ARCHITECTURES

Finding the optimal policy to the proposed infinite-horizon POSG problem is undecidable. Deep neural networks (DNNs) are universal function approximators and can be trained to learn a mapping from data efficiently through gradient descent and backpropagation [35]. Thus, we can use DNNs to approximate the policies and use the agents' experience to learn policies that minimize the cost. This deep MARL has been proven to be successful in many complex multiagent tasks [36]–[40]. However, many of the problems traditionally investigated in the MARL literature can be trained on computer clusters, where the computing nodes are connected together through high-speed network interconnections and can easily share information among themselves to mitigate the partial observability of POSGs [16]. On the other hand, when the computing nodes (in our case MTDs and edge computing infrastructure) are connected via wireless links, sending additional information incurs in an expensive overhead. Therefore, it is imperative to propose novel ways to train these DNNs to solve the POSG problem, while sharing as little information between the computing nodes as possible. For this reason, we chose an actor-critic policy gradient approach [41], as we have more flexibility on distributing the training and inference by placing the actor and the critic on different computing nodes.

In this setting, we propose three different distributed learning architectures: IL, DACC and CLDI. Fig. 2 illustrates the main differences between these architectures. Firstly, in the IL architecture, each MTD has its own network for policy selection (the actor) and value estimation (the critic). Secondly, in the DACC, the value estimator and policy selection networks are decoupled. Each MTD has its own policy selection network and an edge agent, which we assume is connected to every BS and has access to the state of every MTD, stores and trains a value estimator network. At each TTI the edge node feedbacks the critic value of the current state to all MTDs through a broadcast channel. MTDs use the feedback value estimate as the actor-critic's baseline to train their policy selection network. In the CLDI architecture, we follow a similar approach to [38], [39], and consider that the edge node trains the weights (only from local observations) of a single policy network that is shared among all agents and sends it periodically through a broadcast channel. Then, MTDs are able to select their actions only from local observations. Notice that in the DACC and CLDI architectures, the MTDs need to feedback their state information back to the BS. This can be achieved by appending the buffer information to the transmitted packets, or by scheduling periodic state information transmission through a collision free channel. Nevertheless, in this paper, our aim is to evaluate the performance of the proposed architectures, and thus, we assume the state information can be reliably trans-

mitted to the BS. Each approach presents its own advantages and challenges, as detailed in the rest of this section.

In order to provide a fair comparison, in all of the proposed architectures, we consider an actor-critic style PPO algorithm [42], due to its ease of implementation, the possibility of decoupling the policy and the value estimator, reduced sample complexity compared to trust region policy optimization (TRPO) [18], and first-order updates. We start this section by introducing policy gradient methods and the PPO algorithm, and proceed to describe the three proposed architectures in detail.

A. Policy Gradient Methods

In contrast to action-value methods, such as Q-learning [43], where the agent learns an action-value function and derives a policy from selecting the actions that maximize its output, policy gradient methods learn a parametrized policy that selects the actions without consulting a value function. Let $\mathbf{w} \in \mathbb{R}^d$ be the policy parameter vector, then the parametrized policy $\pi_{\mathbf{w}}(a|s) = \mathbb{P}(a|s, \mathbf{w})$ denotes the probability of selecting action a , while at state s with policy parameter \mathbf{w} .

In order to learn the policy parameter vector, we need to have an objective function of \mathbf{w} to be maximized. Consider a scalar performance function $J(\mathbf{w})$, differentiable with respect to \mathbf{w} . Then, the learning procedure consists in maximizing $J(\mathbf{w})$ through gradient ascent updates of the form [41]

$$\mathbf{w}' = \mathbf{w} + \eta \nabla_{\mathbf{w}} \tilde{J}(\mathbf{w}), \quad (17)$$

where η is the learning rate, and $\nabla_{\mathbf{w}} \tilde{J}(\mathbf{w})$ is an estimator of the gradient of the performance measure. A common choice of performance measure is

$$J(\mathbf{w}) = \pi_{\mathbf{w}}(a|s) A_{\pi}(s, a), \quad (18)$$

where $A_{\pi}(s, a) = Q_{\pi}(s, a) - V_{\pi}(s)$ is the advantage function, which gives the advantage of taking action a while at state s in comparison to the state value function, which gives the value of the average action. The state value function for policy π , $V_{\pi}(s)$, is given by the expected discounted reward of state s while following policy π , defined as

$$V_{\pi}(s) = E_{\pi} \left[\sum_{t=0}^{\infty} -\gamma^t c(s_t, a_t) \middle| s_0 = s \right]. \quad (19)$$

Furthermore, the action-value function for policy π , $Q_{\pi}(s, a)$, gives the expected discounted reward of taking action a while in state s and then continuing to follow policy π , which is given as

$$Q_{\pi}(a, s) = E_{\pi} \left[\sum_{t=0}^{\infty} -\gamma^t c(s_t, a_t) \middle| s_0 = s, a_0 = a \right]. \quad (20)$$

Notice that both (19) and (20) can be estimated from experience. This class of algorithms are known as *actor-critic* because we evaluate the difference between the actor estimate ($Q_{\pi}(s, a)$) and the critic estimate ($V_{\pi}(s)$), as presented in (18).

Let $\mathcal{E}_{\pi_{\mathbf{w}}}$ be the set of the experience tuples collected while following policy $\pi_{\mathbf{w}}$, where an experience tuple consists of the state, action, and cost. Then, the gradient of the performance

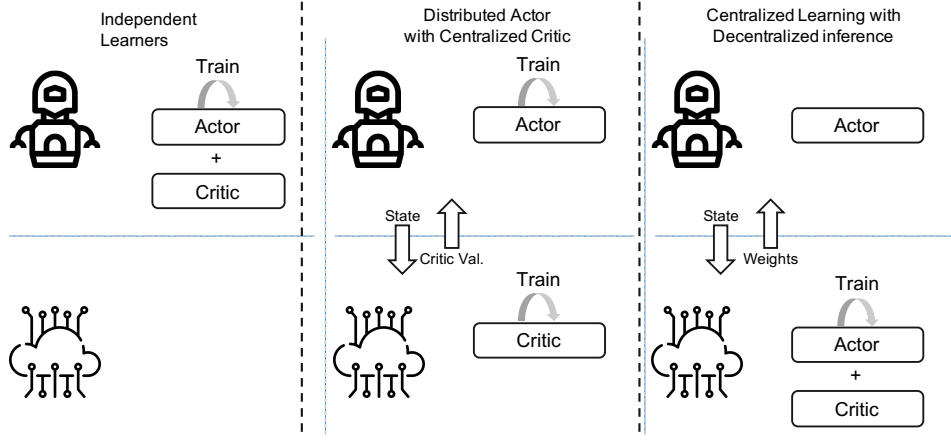


Fig. 2. The diagram illustrates the differences between the three proposed architectures.

measure can be estimated by taking the average gradient over a random finite batch of experience tuples as

$$\nabla_{\mathbf{w}} \tilde{J}(\mathbf{w}) = \hat{E}_{\mathcal{E}_{\pi_{\mathbf{w}}}} [\nabla_{\mathbf{w}} \ln \pi_{\mathbf{w}}(a|s) A(s_t, a_t)], \quad (21)$$

where $\hat{E}_{\mathcal{E}_{\pi_{\mathbf{w}}}}$ denotes the empirical average over a batch of randomly sampled experience tuples.

B. Proximal Policy Optimization

The PPO algorithm, originally proposed in [42], consists in maximizing a clipped surrogate objective $J^{\text{clip}}(\mathbf{w})$ instead of the original performance measure $J(\mathbf{w})$, therefore avoiding the destructively large updates experienced in policy gradient methods without clipping as shown in [42]. The surrogate objective is defined as in (22), shown on the top of the next page, where $\Gamma(\mathbf{w}) = \frac{\pi_{\mathbf{w}}(a|s)}{\pi_{\mathbf{w}_{\text{old}}}(a|s)}$ is the importance weight, ϵ is a hyperparameter that controls the clipping, and \mathbf{w}_{old} are the policy weights prior to the update. Due to the term $\text{clip}(\Gamma(\mathbf{w})A(s, a), 1 - \epsilon, 1 + \epsilon)$ in (22), the importance weight is clipped between $1 - \epsilon$ and $1 + \epsilon$, minimizing the incentives for large destabilizing updates. Furthermore, by taking the minimum of the clipped and unclipped functions, the resulting surrogate objective is a lower bound first-order approximation of the unclipped objective around \mathbf{w}_{old} .

Furthermore, the performance measure is augmented to include a value function loss term, corresponding to the critic output, given by

$$J^{\text{VF}}(\mathbf{w}) = \hat{E}_{\mathcal{E}_{\pi_{\mathbf{w}}}} \left[\left(V_{\pi_{\mathbf{w}}}(s) - \sum_{k=0}^{|\mathcal{E}|-1} \gamma^k r \right)^2 \right]. \quad (23)$$

Finally, a final term of entropy bonus $H(\pi_{\mathbf{w}})$ is added to encourage exploration of the state space [44]. The final surrogate objective function to be maximized is given by

$$J^{\text{sur}}(\mathbf{w}) = J^{\text{clip}}(\mathbf{w}) - k_1 J^{\text{VF}}(\mathbf{w}) + k_2 H(\pi_{\mathbf{w}}), \quad (24)$$

where k_1 and k_2 are system hyperparameters. The PPO algorithm is summarized in Algorithm 1. We use two DNNs, one to approximate the policy $\pi(a|s)$, which takes the state as an input and outputs a probability distribution over \mathcal{A} and the action a is sampled from this distribution. This network is

Algorithm 1: PPO algorithm

Initialization

- 1) Set learning rate $\alpha \in [0, 1]$
- 2) Set the update period T
- 3) Set ϵ, k_1, k_2
- 4) Initialize \mathbf{w}_{old} randomly
- 5) Set $s = s_0 \in \mathcal{S}$
- 6) Set $t \leftarrow 0$

loop

```

 $\mathcal{E} \leftarrow$  Initialize with an empty array of size  $T$ ;
for  $m = 1 \dots T$  do
   $a' \sim \pi_{\mathbf{w}_{\text{old}}}(a|s)$ ;
   $s' \sim \mathbb{P}(s'|s, a)$ ;
   $c' = c(s, a)$ ;
   $\mathcal{E}_m \leftarrow (s, a', c', s')$ ;
end
for  $n = 1 \dots N_{\text{epochs}}$  do
  Sample minibatch  $\tilde{\mathcal{E}}$  from  $\mathcal{E}$  such that  $|\tilde{\mathcal{E}}| < T$ ;
   $\nabla_{\mathbf{w}} \tilde{J}(\mathbf{w}) \leftarrow \hat{E}_{\tilde{\mathcal{E}}} [\nabla_{\mathbf{w}} \ln \pi_{\mathbf{w}}(a|s) A(s_t, a_t)]$ ;
   $\mathbf{w} \leftarrow \mathbf{w}_{\text{old}} + \alpha \nabla_{\mathbf{w}} \tilde{J}^{\text{sur}}(\mathbf{w})$ ;
end
 $\mathbf{w}_{\text{old}} \leftarrow \mathbf{w}$ 
end ;

```

trained to maximize the PPO surrogate performance measure in (24). The second DNN approximates $V_{\pi}(s)$, and is trained to minimize the mean squared error between the output of the network and the average value of the state observed so far. The DNN architecture used by all of the algorithms considered in this paper is described in detail on Appendix B.

C. Independent Learners

In the IL architecture, each device has its own set of weights \mathbf{w}_i and is running its own learning algorithm to update their weights without sharing information about their policies or current and previous states. As each device has only a local view of the state of the environment, it cannot learn the optimal joint-policy in (11). Therefore, each MTD tries to find its local optimal policy as defined on (25), on the top of the next page,

$$J^{\text{clip}}(\mathbf{w}) = \hat{E}_{\mathcal{E}_{\pi_{\mathbf{w}}}}[\min(\Gamma(\mathbf{w})A(s, a), \text{clip}(\Gamma(\mathbf{w}), 1 - \epsilon, 1 + \epsilon)A(s, a))] \quad (22)$$

$$\pi_i^* = \arg \min_{\pi_i \in \Pi_i^{IL}} E_{\mathbf{o}_i \sim \mathbb{P}(\mathbf{o}), \pi_i} \left[\sum_{t=0}^{\infty} \gamma^t c_i(\mathbf{o}_{i,t}, \mathbf{a}_{i,t}) \mid \mathbf{o}_{i,0} = \mathbf{o}_i \right], \quad (25)$$

where $\Pi_i^{IL} = \{\pi \mid \pi : \mathcal{A}_i \times \mathcal{O}_i \rightarrow [0, 1]\}$ is the set of all possible policies mapping the action-observation space into a probability. Notice that the joint policy search space of the IL POSG is $\Pi^{IL} = \Pi_1^{IL} \times \Pi_2^{IL} \times \dots \times \Pi_{N_u}^{IL}$. Additionally, the local cost function is given by

$$c_i(\mathbf{o}_i, \mathbf{a}_i) = x_i(P_{ON} + p_i) + (1 - x_i)P_{OFF} + \omega_i(b_i + \mu_i \xi_i). \quad (26)$$

Consequently, the local cost functions leads to the definition of a local value function

$$V_{\pi_i}^{IL}(o_i) = E_{\pi_i} \left[\sum_{t=0}^{\infty} -\gamma^t c(o_{i,t}, a_{i,t}) \mid o_{i,0} = o_i \right]. \quad (27)$$

Furthermore, the policy function is approximated by a DNN $\pi_{\mathbf{w}_i}$ that is trained on its previous experience using Algorithm 1. As both the policy and value DNNs are trained on the same MTD, both the actor and the critic networks share the same weights to reduce the memory footprint, but have different output heads, the actor head outputs the probabilities of selecting each action, while the critic head outputs critic values. The diagram in Fig. 3 illustrates this architecture.

Effectively, each agent tries to solve the problem defined in (25) while ignoring the effects of other agents, treating it as part of the environment. So, the problem reduces to a Markov decision process (MDP) [29]. The agents change their policies independently of one another, but their actions affect the costs experienced by other agents. Therefore, the agents perceive the environment as non-stationary [40]. To the best of our knowledge, there are no known algorithms that give theoretical guarantees of convergence and optimality in the non-stationary MDP setting nor on the solution of the general POSG problem posed in (11). However, the IL is considered to be a reasonable heuristic to find sub-optimal solutions to a POSG [17]. As shown in Fig 2, the main advantage of this approach is that it does not require any form of communications between devices nor between a device and the BS. On the other hand, it requires every device to have its own set of weights and to run its own learning algorithm, which can result in a high power consumption. Also, as each agent faces a non-stationary environment, there are no guarantees of convergence to an optimal solution.

D. Distributed Actor with Central Critic

The PPO algorithm makes use of two networks: the actor, which models the agent's policy, and the critic, which estimates the value of a state. Originally, the algorithm proposes that both networks can share weights to accelerate convergence and reduce memory costs [42]; In the DACC architecture,

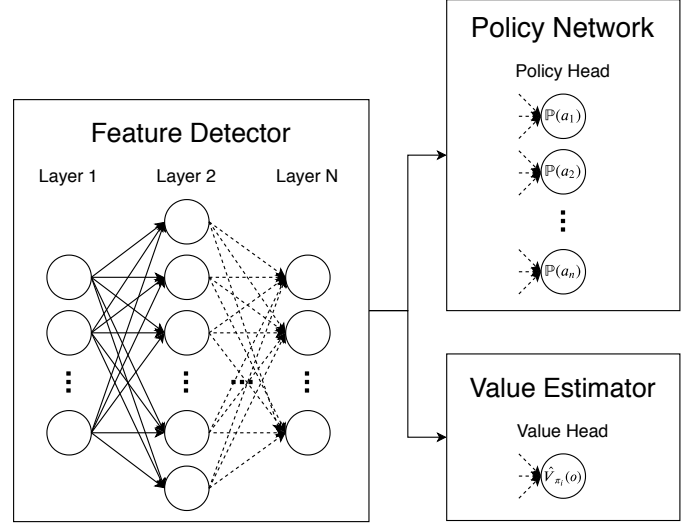


Fig. 3. Diagram of DNN architecture with shared weights and split actor and critic heads.

each agent learns its own policy based on its local cost, similar to the IL architecture, while a single critic is stored and trained on an edge computing node. The goal of this architecture is to mitigate the effects of the partial observation by having a critic that has access to the data of all the agents (the whole state) to estimate the value of the whole state \mathbf{s} , defined in (19), and not only the local value based on the local observations as done by the IL architecture. Thus, the DACC POSG problem is given by (28), located on top of next page, where $\Pi_i^{DACC} = \{\pi \mid \pi : \mathcal{A}_i \times \mathcal{O}_i \rightarrow [0, 1]\}$ is the set of all possible probability distributions over the action-observation space, and the joint policy search space of the DACC POSG is $\Pi^{DACC} = \Pi_1^{DACC} \times \Pi_2^{DACC} \times \dots \times \Pi_{N_u}^{DACC}$. While the critic value is computed on local observation data in the IL architecture, as shown in (27), the critic value in the DACC architecture is computed over global state information, i.e. $V_{\pi}^{DACC}(\mathbf{s}) = V_{\pi}(\mathbf{s})$.

Both the policy function π_i and the value function estimator $V_{\pi}^{DACC}(\mathbf{s})$ are approximated by DNNs. The policy DNN $\pi_{\mathbf{w}_i}$ is trained and stored on each device, while the value function estimator is stored and computed on an edge computing node. Hence, in this architecture, the surrogate objective function in (24) is split into two, with one to be minimized by the devices to train the policy network, given by

$$J_a^{\text{sur}}(\mathbf{w}_i) = J^{\text{clip}}(\mathbf{w}_i) + k_2 H(\pi_{\mathbf{w}_i}), \quad (29)$$

and the other to be minimized on the edge to train the value

$$\pi_i^* = \arg \min_{\pi_i \in \Pi_i^{PACC}} E_{\mathbf{o}_i \sim \mathbb{P}(\mathbf{o}), \pi_i} \left[\sum_{t=0}^{\infty} \gamma^t c_i(\mathbf{o}_{i,t}, \mathbf{a}_{i,t}) \mid \mathbf{o}_{i,0} = \mathbf{o}_i \right], \quad (28)$$

function network, given by

$$J_c^{\text{sur}}(\mathbf{w}_c) = J^{\text{VF}}(\mathbf{w}_c). \quad (30)$$

Furthermore, as illustrated in Fig. 2, each agent keeps its own set of weights \mathbf{w}_i for the actor network, while the weights of the value function estimator \mathbf{w}_c are stored and updated on the edge computing node. Additionally, both the MTDs and the edge node must perform backpropagation to update their weights. While each MTD has access to its own local information, the value estimator trained on the edge can leverage the data collected by all agents, and thus, the edge agent is able to backpropagate on the global state information.

Moreover, as shown in (21), the critic value is necessary to compute the PPO gradient. Therefore, this architecture requires the BSs to feedback the value of each state, $V_{\pi}(\mathbf{s})$ given in (19), after every TTI, such that the agents are able to perform backpropagation and train their policy networks. Moreover, while the channel response can be estimated by the network from the preambles, the buffer occupancy information b_i needs to be sent by the MTDs to the edge in every TTI, thus, the edge node is able to compute the value functions and its weight's update.

E. Centralized Learning with Distributed Inference

As the number of MTDs in the network increases, the size of the policy search space for the IL and DACC architectures increase exponentially, consequently increasing the solution space. To address this issue, in the CLDI architecture, there is a single set of weights, and therefore a single policy π and a search space $\Pi^{\text{CLDI}} = \{\pi | \pi : \mathcal{A}_i \times \mathcal{O}_i \rightarrow [0, 1], i = 1, \dots, N_U\}$ that does not increase in size with the number of MTDs. Both the policy and the critic are trained on the edge and an updated set of weights is periodically broadcast to the MTDs, thus reducing the computational burden required to train a neural network on the devices. Moreover, the policy on the edge is trained on data from all MTDs leading to improved sample efficiency. Hence, instead of solving (11), the CLDI architecture looks for solutions to (31), defined on the top of the following page, where the CLDI cost function is given by

$$c_{\text{CLDI}}(\mathbf{s}, \mathbf{a}) = \frac{1}{N_U} \sum_{i=1}^{N_U} x_i(P_{ON} + p_i) + (1 - x_i)P_{OFF} + \omega_i(b_i + \mu_i \xi_i), \quad (32)$$

which is the average cost function of the MTDs. It is worth highlighting that the CLDI cost is an average of the costs of all MTDs, thus, the shared policy is updated to increase the average performance of all MTDs, as opposed to the IL and the DACC architecture where the policy of each MTD is updated to optimize its local performance. Both the policy and value function networks are stored and trained on the

TABLE I
PARAMETERS USED IN THE SIMULATIONS

Parameter	Value	Parameter	Value
f_S	10^5 symbols/s	L	100 bytes
R	300 m	Δ_t	10 ms
N_U	{2560, 7680} users	δ_i	$U(\{4, 8, 12\})$ packets
N_B	2 BS	λ_i	$U(\{40, 60, 80\})$ packets/s
N_S	8 subcarriers	γ	0.99
N_P	64 preambles	P_{ON}	320 milliwatts
α	3.5	P_{OFF}	0 milliwatts
B	25 packets	f_{\max}	10 Hz
T	200 TTI		

edge following Algorithm 1 using the cost function defined in (32). The devices have a copy of the policy network, but they do not train it, they just use it for decision-making. In this architecture, the devices must append the buffer state information to every transmitted packet, and thus, the networks can be trained on the edge node, where the network must send the updated weights back to the MTDs periodically.

IV. NUMERICAL EXPERIMENTS

In this section, the performance of the proposed architectures is evaluated through computer simulations. In order to provide a frame of reference, we also simulate the performance of a baseline employing a reactive HARQ protocol with power boosting. The details of the baseline are described in Appendix A. We consider that there are two BSs and eight subcarriers serving a circular area with a 300 m radius. We generate 1000 realizations of this scenario, where at each realization we place both the BSs and the MTDs in a random location within the circular area. At each realization the learning algorithms start from scratch (e.g. the weights of the agents are randomly initialized at the beginning of each realization) and runs for 15000 TTI. Then, we compare the average performances, along with their variances, with respect to the average delay experienced by the network, the number of dropped packets, the average power spent, and the number of collisions.

A. Results

We compare the baseline and the architectures proposed in Section III in terms of the average network delay, power, dropped packets, and collisions during 15000 TTIs. We evaluate the network delay through the holding cost, as the average network delay is proportional to the number of packets held in the devices' buffer. We consider that devices with different mean packet arrival rates and latency constraints are being serviced by the same cellular network. For each realization, the packet arrival rate of each MTDs is uniformly sampled from {40, 60, 80} packets per second and the latency constraint is uniformly sampled from {4, 8, 12} queued packets. Notice that in all the plots the x -axis shows the TTI. In the holding cost plot, the y -axis shows the cumulative average of the number

$$\pi^* = \arg \min_{\pi \in \Pi^{CLDI}} E_{\mathbf{s} \sim \mathbb{P}(\mathbf{s}), \pi} \left[\sum_{t=0}^{\infty} \gamma^t c_{CLDI}(\mathbf{s}_t, \mathbf{a}_t) \mid \mathbf{s}_0 = \mathbf{s} \right], \quad (31)$$

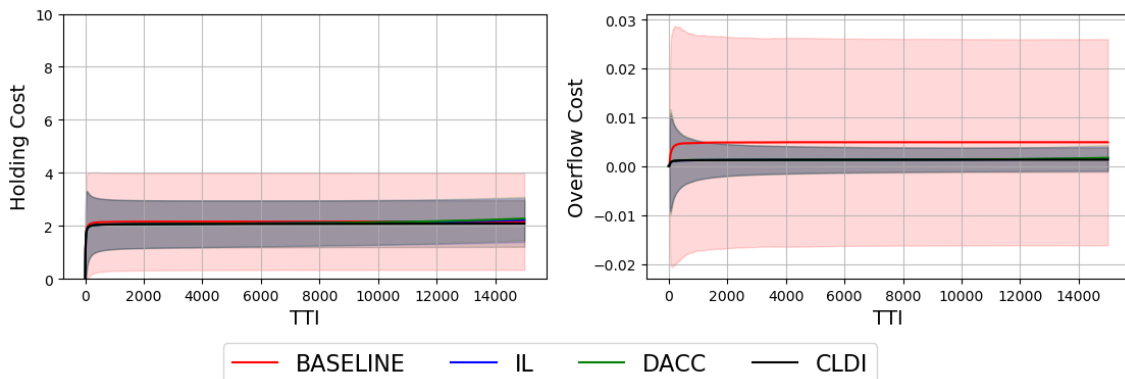


Fig. 4. Simulation results showing the holding costs and overflow costs with 2560 MTDs in the simulated area for the three proposed architectures and the baseline, where IL stands for the independent learners, DACC for distributed actor with central critic and CLDI for central learning with decentralized inference.

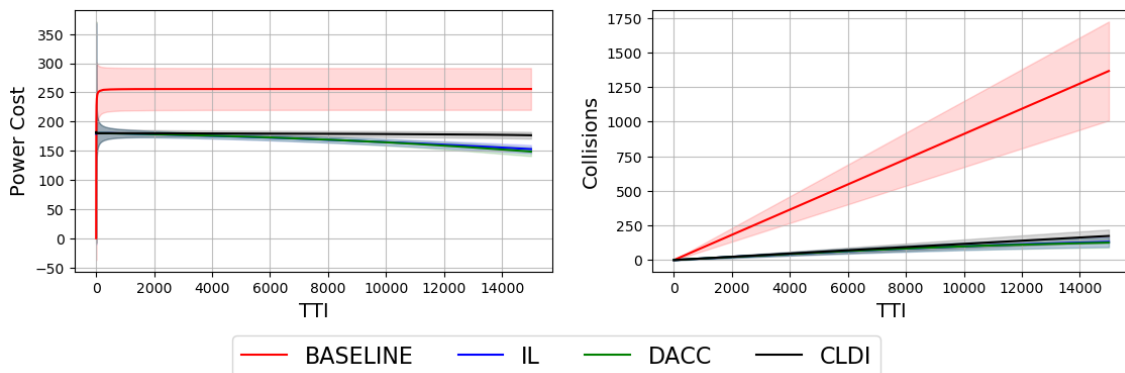


Fig. 5. Simulation results showing the power costs and the number of collisions with 2560 MTDs in the simulated area for the three proposed architectures and the baseline, where IL stands for the independent learners, DACC for distributed actor with central critic and CLDI for central learning with decentralized inference.

of packets in the buffer at a given TTI. The y -axis in the overflow cost plots show the cumulative average value of ζ_i . Furthermore, the y -axis in the power cost plots shows the cumulative average of the power spent by MTDs in milliwatts. Finally, the y -axis in the collisions' plot shows the cumulative sum of collisions up to the given TTI.

As shown in Fig. 4, with 2560 users, the average holding cost between all four approaches is roughly the same. However, we notice that the baseline presents a significantly higher variance than the proposed architectures. Furthermore, the average network delay is below four, which is the smallest latency constraint in the network, within at least one standard deviation. With respect to overflow packets, also in Fig. 4, on average the baseline approach drops slightly more packets than the proposed architectures, but again with significantly more variance. With respect to the power consumption, as shown in Fig. 5, the three proposed architectures spend on average roughly 70% of the power spent by the baseline. Moreover, as mentioned in Section III, the CLDI algorithm tends to converge faster as it is trained on observations from

every device in the network and has to search for a policy in a notably small policy search space. This is confirmed by the fact that, as the simulation advances in time and the IL and DACC algorithms train on more data, they achieve similar performance levels as CLDI, while using less power. The performance improvement of the proposed architectures compared to the baseline is even more significant when it comes to the number of collisions, as shown in Fig. 5. On average, the reinforcement learning based solutions experience 15% of the baseline's collisions during the same period of time.

Moreover, in all investigated architectures, the holding cost performance, when averaged over users with the same delay constraint, follows the same trend as when averaged over all users (shown in Fig. 4). Therefore, we can conclude that in a scenario with 2560 MTDs, in average, all the architectures satisfy the delay constraints. However, the baseline approach presents larger performance fluctuations, as shown by the larger standard deviation in Fig. 4.

As illustrated in Fig. 6, when the number of users is

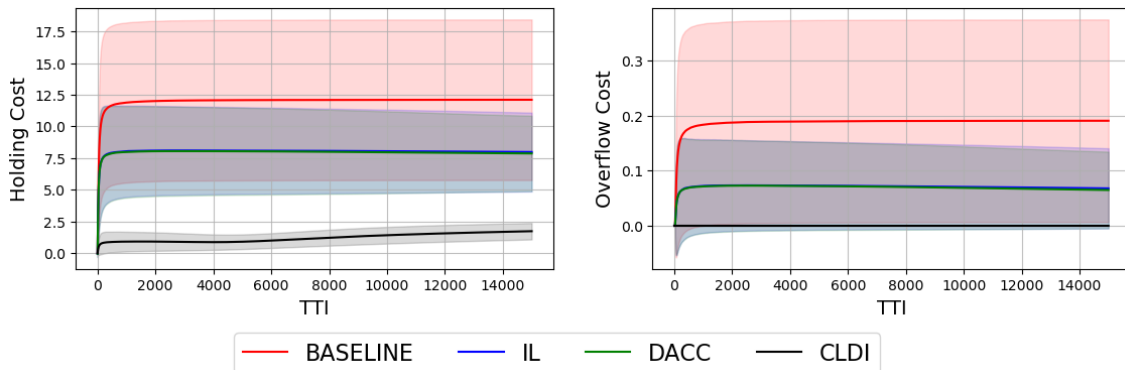


Fig. 6. Simulation results showing the holding costs and overflow costs with 7680 MTDs in the simulated area for the three proposed architectures and the baseline, where IL stands for the independent learners, DACC for distributed actor with central critic and CLDI for central learning with decentralized inference.

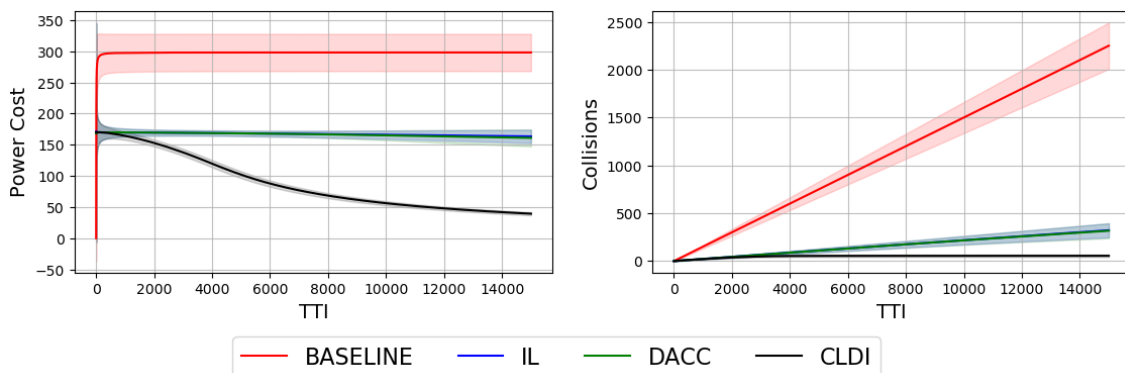


Fig. 7. Simulation results showing the power costs and the number of collisions with 7680 MTDs in the simulated area for the three proposed architectures and the baseline, where IL stands for the independent learners, DACC for distributed actor with central critic and CLDI for central learning with decentralized inference.

increased to 7680, the average holding cost of the CLDI architecture converges to 2 packets, while the IL and DACC converge to 8 packets and the baseline to 12 packets. From this result, we conclude that as the number of users increases the lack of collaboration between the MTDs in the IL and DACC architectures starts to impact the average network delay, while CLDI performance stays around the same as for 2560 users. Also in Fig. 6, the average overflow cost of CLDI still remains around 0, while the IL and DACC stabilize around 0.7 and the baseline at 0.19. With regards to the average power costs at convergence, the CLDI architecture spends 16.66% of the power spent by the baseline, while the IL and DACC spend 52%, as seen in Fig. 7. The significant decrease in the power spent by CLDI is explained by the centralized training, which makes more training data available, since CLDI has 7680 new data points for each TTI while the other architectures have only 1, which points to a cooperative behavior arising among the MTDs. This is also reflected in the collisions performance, where CLDI experiences around 2.25% of the baseline's collisions and IL and DACC experience around 14%.

Furthermore, similar to the 2560 MTDs case, in all architectures investigated, all devices converge to roughly the same average holding cost, regardless of the delay constraint.

Thus, in the 7680 MTDs scenario, only the CLDI architecture maintains an average holding cost below the delay constraints for devices with $\delta_i = 4$, $\delta_i = 8$ and $\delta_i = 12$. In the IL and DACC architectures, in average, only devices with $\delta_i = 8$ and $\delta_i = 12$ satisfy their constraints. Finally, when the baseline architecture is employed, on average, none of the MTDs is able to satisfy its constraint. This confirms that the CLDI architecture scales better than the others in densely deployed scenarios.

B. Tradeoffs

In this subsection, we analyze the advantages and disadvantages of each of the proposed architectures, and discuss possible application scenarios.

The IL architecture does not require a central edge entity to work, and therefore it cuts all the necessary overhead associated to data transmission between MTDs and BSs. However, each MTD has to perform training and inference of its DNN, which can be computationally expensive. Moreover, as each MTD is trained in a fully distributed manner, without sharing any information, there is no chance of cooperation arising. Both DACC and CLDI architectures require MTDs to transmit information about their number of packets currently in the buffers. On the other hand, since part of the training for

TABLE II
OVERHEAD AND PERFORMANCE TRADEOFFS FOR $N_U = 2560$

Algorithm	DL Overhead	UL Overhead	Collisions	Power Cost	Holding Cost
Baseline	-	-	1364 collisions	255.54 mW	2.15 packets
IL	-	-	131 collisions	168.68 mW	2.11 packets
DACC	1.6 kbits/s	1.6 kbits/s	122 collisions	168.06 mW	2.12 packets
CLDI	20.496 kbits/s	1.6 kbits/s	174 collisions	178.81 mW	2.07 packets

TABLE III
OVERHEAD AND PERFORMANCE TRADEOFFS FOR $N_U = 7680$

Algorithm	DL Overhead	UL Overhead	Collisions	Power Cost	Holding Cost
Baseline	-	-	2253 collisions	297.6154 mW	12.01 packets
IL	-	-	322 collisions	166.98 mW	8.025 packets
DACC	1.6 kbits/s	1.6 kbits/s	317 collisions	166.25 mW	7.95 packets
CLDI	20.496 kbits/s	1.6 kbits/s	55 collisions	87.81 mW	1.21 packets

DACC, and all the training for CLDI is performed in the edge, some of the computational burden is offloaded, thus saving power and easing the computation requirements of MTDs. In this work, we use 16 bit floating point numbers to encode the state information, action, and network weights. Furthermore, we consider any extra data exchange that is not the payload to be overhead. Thus, in the uplink direction, the overhead of the DACC and CLDI architectures is given by $\frac{16}{\Delta_t}$. Regarding the downlink overhead, in the DACC architecture the network must send the critic value in every TTI, and therefore, the overhead is also $\frac{16}{\Delta_t}$. Meanwhile, in the CLDI architecture, the network must send all the weights of the DNN to the MTDs every 200 TTI.

Tables II and III show the average performance of each architecture and its respective overhead. As shown in Section IV-A, for a smaller user density, the IL and DACC architectures slightly outperform CLDI. However, for a higher density of MTDs, the CLDI architecture is able to leverage data from observations collected from all MTDs, and thanks to the centralized training, the MTDs work together to use the network resources more equitably, resulting in tremendous power savings, small average delays, and a minimal number of dropped packets and collisions. Therefore, we conclude that for cellular networks designed to serve a smaller number of MTDs, the IL and DACC architectures, depending on whether the devices have enough computational power to train their DNN and how much overhead is tolerated, are recommended. However, for cellular networks designed to support a massive number of low-cost devices, the CLDI architecture is deemed more suitable.

V. CONCLUSIONS

In this paper, we proposed a system model for mMTC networks using grant-free transmission and formulated it as an average power minimization problem subject to delay constraints. Based on the related literature, we conclude that static access protocols are inefficient to handle the optimization problem and proposed three reinforcement learning based architectures to solve the optimization problem in a distributed fashion. The architectures have different degrees of centralization and overhead. Furthermore, we simulated the three

architectures and compared their performance among against a static access policy baseline based on the reactive HARQ protocol with power boosting. Finally, we showed that all three learnable architectures outperform the static baseline and we proceeded to analyze the tradeoffs between the architectures.

APPENDIX A BASELINE ALGORITHM

Firstly, each device with packets in the buffer to transmit draws a random number $q \sim U([0, 1])$, and if $q \leq \bar{q}$, where \bar{q} is a congestion control threshold, the device tries to access the channel. This is done to avoid congestion by having all devices trying to access the channel at the same time. Furthermore, if the MTD is currently violating its delay constraints or if there was a dropped packet in the last TTI, the device ramps up its power. Moreover, if at least one packet was successfully transmitted on the last TTI, the MTD assumes it is facing a good channel condition, and it then increases the transmission modulation order. Otherwise, it assumes a bad channel and decreases it. The algorithm is described by the flowchart in Fig. 8.

APPENDIX B DNN ARCHITECTURE AND PARAMETERS

One of the requirements is that the DNN must be shallow and relatively small to keep a light memory footprint on the devices and to reduce the computational complexity of the training and inference. We consider a GRU [45] connected to a two-layer perceptron. As the observations of the MTDs are temporally correlated (through the number of packets in the buffer, and the channel gains) we include a GRU in the input to extract information from sequences of states. We employ GRUs as it has been shown that they have comparable performance to the more commonly used long short term memory (LSTM) units while being more computationally efficient [46]. In our model, we consider a GRU with $N_B N_S + 4$ inputs, where $N_B N_S$ inputs take the channel state information, and the remaining four are the number of packets in the buffer (b_i), the number of arriving packets (l_i), the goodput on the previous TTI (g_i) and the number of overflowed packets in the

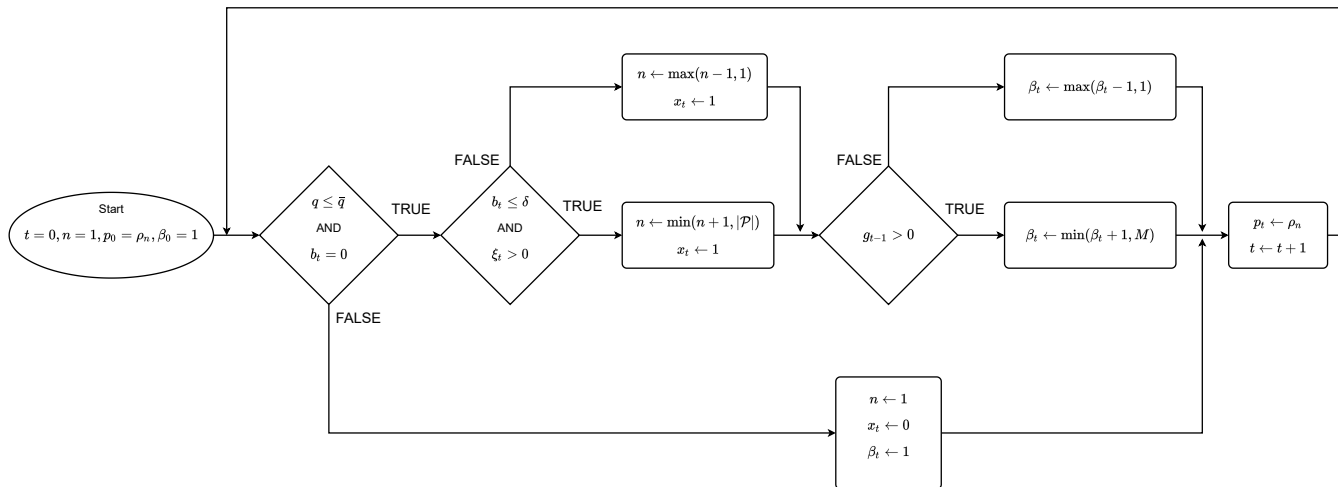


Fig. 8. Flowchart of the baseline algorithm.

TABLE IV
NUMBER OF WEIGHTS IN THE DNN

Gated Recurrent Unit (GRU)	Fully Connected Layers	Policy Network Head	Value Function Network Head
$3[32^2 + 32(4 + N_B N_S) + 32]$	2×32^2	$322M \mathcal{P} N_S$	32

previous TTI (ξ_i). The GRU unit has 32 output values, while both of the linear layers have 32 inputs and 32 outputs. Finally, the actor head has 32 inputs and $2M|\mathcal{P}|N_S$ outputs (one for each possible action), while the critic head has 32 inputs and one output (the critic value). Table IV summarize the number of weights needed for each stage of the network¹.

The networks are trained using an adaptive moment estimation (ADAM) optimizer [48] with a learning rate of 7×10^{-4} . At each DNN network update, the weights are trained over 4 PPO epochs with 10 minibatches per epoch. To avoid large gradient updates that make the optimization unstable, the gradients are clipped such that $\|\nabla J_w\| \leq 0.5$. A value loss coefficient $k_1 = 0.5$ and an entropy loss coefficient $k_2 = 0.01$ are used.

REFERENCES

- [1] Machina Research, "M2M growth necessitates a new approach to network planning and optimisation," Machina Research, Tech. Rep., May 2015.
- [2] Y. Gao and L. Dai, "Random access: Packet-based or connection-based?" *IEEE Trans. Wireless Commun.*, vol. 18, no. 5, pp. 2664–2678, May 2019.
- [3] K. Au, L. Zhang, H. Nikopour, E. Yi, A. Bayesteh, U. Vilaipornsawai, J. Ma, and P. Zhu, "Uplink contention based SCMA for 5G radio access," in *IEEE Globecom Workshops*, Dec 2014, pp. 900–905.
- [4] C. Hoymann, D. Astely, M. Stattin, G. Wikstrom, J. Cheng, A. Hoglund, M. Frenne, R. Blasco, J. Huschke, and F. Gunnarsson, "LTE release 14 outlook," *IEEE Commun. Mag.*, vol. 54, no. 6, pp. 44–49, June 2016.
- [5] 3GPP, "Physical layer procedures for control," 3rd Generation Partnership Project (3GPP), Technical Specification (TS) 38.213, Apr 2018, version 16.5.0.
- [6] 3GPP, "TR 38.192 - study on new radio (NR) access technology," 3GPP, Tech. Rep., 2017.
- [7] L. Liu, E. G. Larsson, W. Yu, P. Popovski, C. Stefanovic, and E. de Carvalho, "Sparse signal processing for grant-free massive connectivity: A future paradigm for random access protocols in the internet of things," *IEEE Signal Process. Mag.*, vol. 35, no. 5, pp. 88–99, Sep. 2018.
- [8] C. Bockelmann, N. Pratas, H. Nikopour, K. Au, T. Svensson, C. Stefanovic, P. Popovski, and A. Dekorsy, "Massive machine-type communications in 5G: physical and MAC-layer solutions," *IEEE Commun. Mag.*, vol. 54, no. 9, pp. 59–65, Sep. 2016.
- [9] J. V. C. Evangelista, Z. Sattar, and G. Kaddoum, "Analysis of contention-based SCMA in mMTC networks," in *IEEE Latin-American Conference on Communications (LATINCOM)*, 2019, pp. 1–6.
- [10] J. Liu, G. Wu, X. Zhang, S. Fang, and S. Li, "Modeling, analysis, and optimization of grant-free NOMA in massive MTC via stochastic geometry," *arxiv e-prints*, Apr. 2020.
- [11] R. Abreu, T. Jacobsen, G. Berardinelli, K. Pedersen, I. Z. Kovács, and P. Mogensen, "Power control optimization for uplink grant-free URLLC," in *IEEE Wireless Communications and Networking Conference (WCNC)*, 2018, pp. 1–6.
- [12] A. Jacquelin, M. Vilgelm, and W. Kellerer, "Grant-free access with multipacket reception: Analysis and reinforcement learning optimization," in *Conference on Wireless On-demand Network Systems and Services (WONS)*, 2019, pp. 83–90.
- [13] R. Huang, V. W. S. Wong, and R. Schober, "Throughput optimization in grant-free NOMA with deep reinforcement learning," in *IEEE Global Communications Conference (GLOBECOM)*, 2019, pp. 1–6.
- [14] N. Mastrorarde and M. van der Schaar, "Joint physical-layer and system-level power management for delay-sensitive wireless communications," *IEEE Trans. Mobile Comput.*, vol. 12, no. 4, pp. 694–709, Apr. 2013.
- [15] N. Mastrorarde, J. Modares, C. Wu, and J. Chakareski, "Reinforcement Learning for Energy-Efficient Delay-Sensitive CSMA / CA Scheduling," in *IEEE Global Communications Conference*, 2016, pp. 1–7.
- [16] C. Claus and C. Boutilier, "The dynamics of reinforcement learning in cooperative multiagent systems," in *Proceedings of the Fifteenth National/Tenth Conference on Artificial Intelligence/Innovative Applications of Artificial Intelligence*. American Association for Artificial Intelligence, 1998, pp. 746–752.
- [17] L. Matignon, G. J. Laurent, and N. Le Fort-Piat, "Independent reinforcement learners in cooperative Markov games: A survey regarding coordination problems," *Knowl. Eng. Rev.*, vol. 27, no. 1, pp. 1–31, Feb 2012.
- [18] J. Schulman, S. Levine, P. Abbeel, M. Jordan, and P. Moritz, "Trust Region Policy Optimization," in *International Conference on Machine Learning*, 6 2015, pp. 1889–1897.

¹We used the values in [47] to compute the number of weights needed by a GRU.

- [19] N. H. Mahmood, R. Abreu, R. Böhnke, M. Schubert, G. Berardinelli, and T. H. Jacobsen, "Uplink grant-free random access solutions for URLLC services in 5G New Radio," 2019.
- [20] J. V. C. Evangelista, Z. Sattar, G. Kaddoum, and A. Chaaban, "Fairness and sum-rate maximization via joint subcarrier and power allocation in uplink SCMA transmission," *IEEE Trans. Wireless Commun.*, vol. 18, no. 12, pp. 5855–5867, 2019.
- [21] M. Patzold, *Mobile Radio Channels*. Wiley Publishing, 2012.
- [22] E. Dahlman, S. Parkvall, and J. Skold, *5G NR: The Next Generation Wireless Access Technology*, 1st ed. USA: Academic Press, Inc., 2018.
- [23] J. Kim, J. Yi, and S. Bahk, "Uplink channel access enhancement for cellular communication in unlicensed spectrum," *IEEE Access*, vol. 8, pp. 216 386–216 397, Nov 2020.
- [24] R. Maldonado, C. Rosa, and K. I. Pedersen, "Latency and reliability analysis of cellular networks in unlicensed spectrum," *IEEE Access*, vol. 8, pp. 49 412–49 423, Mar 2020.
- [25] H. Song, Q. Cui, Y. Gu, G. L. Stüber, Y. Li, Z. Fei, and C. Guo, "Cooperative LBT design and effective capacity analysis for 5G NR ultra dense networks in unlicensed spectrum," *IEEE Access*, vol. 7, pp. 50 265–50 279, Apr 2019.
- [26] M. Heusse, F. Rousseau, G. Berger-Sabbatel, and A. Duda, "Performance Anomaly of 802.11b," in *IEEE International Conference on Computer Communications*. San Francisco, CA, USA: IEEE, 2003, pp. 836–843.
- [27] J. G. Proakis, *Digital Communications*. McGraw-Hill, 2007.
- [28] A. Neyman and S. Sorin, *Stochastic Games and Applications*. Kluwer Academic Publishers, 2003.
- [29] M. L. Puterman, *Markov decision processes: discrete stochastic dynamic programming*. John Wiley & Sons, 2014.
- [30] F. A. Oliehoek and C. Amato, *A Concise Introduction to Decentralized POMDPs*. Springer Publishing Company, Incorporated, 2016.
- [31] O. Madani, S. Hanks, and A. Condon, "On the undecidability of probabilistic planning and infinite-horizon partially observable markov decision problems," in *AAAI '99/IAAI '99*. USA: American Association for Artificial Intelligence, 1999, p. 541–548.
- [32] E. Altman, *Constrained Markov Decision Processes*. Chapman and Hall, 1999.
- [33] J. Nocedal and S. J. Wright, *Numerical Optimization*, 2nd ed. New York, NY, USA: Springer, 2006.
- [34] M. El-Taha and S. Stidham Jr., *Sample-Path Analysis of Queueing Systems*. Springer Science & Business Media, 2012.
- [35] I. Goodfellow, Y. Bengio, and A. Courville, *Deep Learning*, 1st ed. MIT Press, 2016. [Online]. Available: <http://www.deeplearningbook.org>
- [36] J. Foerster, I. A. Assael, N. de Freitas, and S. Whiteson, "Learning to communicate with deep multi-agent reinforcement learning," in *Advances in Neural Information Processing Systems*, D. Lee, M. Sugiyama, U. Luxburg, I. Guyon, and R. Garnett, Eds., vol. 29. Curran Associates, Inc., 2016.
- [37] J. Foerster, N. Nardelli, G. Farquhar, T. Afouras, P. H. S. Torr, P. Kohli, and S. Whiteson, "Stabilising Experience Replay for Deep Multi-Agent Reinforcement Learning," in *ICML 2017: Proceedings of the Thirty-Fourth International Conference on Machine Learning*, Sydney, NSW, Australia, 2017, pp. 1146–1155. [Online]. Available: <http://arxiv.org/abs/1702.08887>
- [38] J. Foerster, G. Farquhar, T. Afouras, N. Nardelli, and S. Whiteson, "Counterfactual multi-agent policy gradients," in *Neural Information Processing Systems*. Advances in neural information processing systems, 2018, pp. 2974–2982.
- [39] R. Lowe, Y. Wu, A. Tamar, J. Harb, and P. Abbeel, "Multi-agent actor-critic for mixed cooperative-competitive environments," in *Neural Information Processing Systems*. Advances in neural information processing systems, 2017, pp. 6379–6390.
- [40] S. Omidshafiei, J. Papis, C. Amato, J. P. How, and J. Vian, "Deep Decentralized Multi-task Multi-Agent Reinforcement Learning under Partial Observability," in *International Conference on Machine Learning*, vol. 70, 2017, pp. 2681–2690.
- [41] R. S. Sutton and A. G. Barto, *Reinforcement Learning: An Introduction*, 2nd ed. Cambridge (Mass.): The MIT Press, 2018.
- [42] J. Schulman, F. Wolski, P. Dhariwal, A. Radford, and O. Klimov, "Proximal Policy Optimization Algorithms," in *arXiv*, 2005, pp. 1–12.
- [43] C. J. C. H. Watkins and P. Dayan, "Q-learning," *Machine Learning*, vol. 8, no. 3-4, pp. 279–292, 1992.
- [44] V. Mnih, A. P. Badia, M. Mirza, A. Graves, T. Lillicrap, T. Harley, D. Silver, and K. Kavukcuoglu, "Asynchronous Methods for Deep Reinforcement Learning," in *Proceedings of Machine Learning Research*. International Conference on Machine Learning, 6 2016, pp. 1928–1937.
- [45] K. Cho, B. van Merriënboer, D. Bahdanau, and Y. Bengio, "On the properties of neural machine translation: Encoder–decoder approaches," in *Proceedings of SSST-8, Eighth Workshop on Syntax, Semantics and Structure in Statistical Translation*. Doha, Qatar: Association for Computational Linguistics, Oct. 2014, pp. 103–111.
- [46] J. Chung, Ç. Gülçehre, K. Cho, and Y. Bengio, "Empirical evaluation of gated recurrent neural networks on sequence modeling," *arXiv e-prints*, vol. abs/1412.3555, 2014, presented at the Deep Learning workshop at NIPS2014.
- [47] R. Dey and F. M. Salem, "Gate-variants of gated recurrent unit (GRU) neural networks," in *IEEE 60th International Midwest Symposium on Circuits and Systems (MWSCAS)*, Aug 2017, pp. 1597–1600.
- [48] D. P. Kingma and J. Ba, "Adam: A method for stochastic optimization," 2017.